SANDIA REPORT
SAND2010-7369
Unlimited Release
Printed October 2010

4-wave mixing for phase-matching free nonlinear optics in quantum cascade structures

Weng Chow, Mike Wanke, Dan Allen, Zhenshan Yang and Ines Waldmueller

Prepared by
Sandia National Laboratories
Albuquerque, New Mexico 87185 and Livermore, California 94550

Sandia National Laboratories is a multi-program laboratory managed and operated by Sandia Corporation, a wholly owned subsidiary of Lockheed Martin Corporation, for the U.S. Department of Energy's National Nuclear Security Administration under contract DE-AC04-94AL85000.

Approved for public release; further dissemination unlimited.

Sandia National Laboratories

Issued by Sandia National Laboratories, operated for the United States Department of Energy by Sandia Corporation.

NOTICE: This report was prepared as an account of work sponsored by an agency of the United States Government. Neither the United States Government, nor any agency thereof, nor any of their employees, nor any of their contractors, subcontractors, or their employees, make any warranty, express or implied, or assume any legal liability or responsibility for the accuracy, completeness, or usefulness of any information, apparatus, product, or process disclosed, or represent that its use would not infringe privately owned rights. Reference herein to any specific commercial product, process, or service by trade name, trademark, manufacturer, or otherwise, does not necessarily constitute or imply its endorsement, recommendation, or favoring by the United States Government, any agency thereof, or any of their contractors or subcontractors. The views and opinions expressed herein do not necessarily state or reflect those of the United States Government, any agency thereof, or any of their contractors.

Printed in the United States of America. This report has been reproduced directly from the best available copy.

Available to DOE and DOE contractors from
U.S. Department of Energy
Office of Scientific and Technical Information
P.O. Box 62
Oak Ridge, TN 37831

Telephone: (865) 576-8401
Facsimile: (865) 576-5728
E-Mail: reports@adonis.osti.gov
Online ordering: http://www.osti.gov/bridge

Available to the public from
U.S. Department of Commerce
National Technical Information Service
5285 Port Royal Rd.
Springfield, VA 22161

Telephone: (800) 553-6847
Facsimile: (703) 605-6900
E-Mail: orders@ntis.fedworld.gov
Online order: http://www.ntis.gov/help/ordermethods.asp?loc=7-4-0#online

SAND2010-7369
Unlimited Release
Printed October 2010

4-wave mixing for phase-matching free nonlinear optics in quantum cascade structures

LDRD 08-0346 Final Report

Weng Chow, Zhenshan Yang and Ines Waldmueller
Semiconductor Material and Device Sciences Department

Mike Wanke and Dan Allen
Photonic Microsystems Technologies Department

Sandia National Laboratories
P.O. Box 5800
Albuquerque, New Mexico 87185-MS1085

Abstract

This report summarizes a 3-year LDRD program at Sandia National Laboratories exploring optical nonlinearities in intersubband devices. Experimental and theoretical investigations were made to develop a fundamental understanding of light-matter interaction in a semiconductor system and to explore how this understanding can be used to develop mid-IR to THz emitters and nonclassical light sources.

ACKNOWLEDGMENTS

The authors would like to acknowledge the helpful technical discussions with Anna Tauke-Pedretti, Eric Shaner and Brandon Passmore, of Sandia National Laboratories as well as Andreas Knorr, Alexander Carmele and Julia Kabuss of the Technical University, Berlin.

CONTENTS

1. Introduction 7
2. Approach 7
3. Results 8
4. References 9

Appendix A: FTIR measurements of V121049 (DASPMT02a) wide barrier photo-current multiplie 10

Appendix B: Photoconductivity of VB0349 (Digital superlattice OPED)……..19

Appendix C: Photoconductivity measurements of a wide barrier photo-current multiplier……..22

Appendix D: Summary of invention disclosures……...27

Appendix E: List of invited talks, contributed talks and TAs……29

Appendix F: Final Briefing……31

Distribution 36

FIGURES

Figure 1. 4-wave mixing…….8
Figure 2. Quantum coherence……..8
Figure 3. 4-level QC structure ……..8

NOMENCLATURE

DOE	Department of Energy
SNL	Sandia National Laboratories
DBR	Distributed Bragg Reflector

1. Introduction

Optical nonlinearities and quantum coherences have the potential to enable efficient, high-temperature generation of coherent THz radiation. This LDRD proposal involves the exploration of the underlying physics using intersubband transitions in a quantum cascade structure. Success in the device physics aspect will give Sandia the state-of-the-art technology for high-temperature THz quantum cascade lasers. These lasers are useful for imaging and spectroscopy in medicine and national defense.

Success may have other far-reaching consequences. Results from the in-depth study of coherences, dephasing and dynamics will eventually impact the fields of quantum computing, optical communication and cryptology, especially if we are successful in demonstrating entangled photons or slow light. An even farther reaching development is if we can show that the QC nanostructure, with its discrete atom-like intersubband resonances, can replace the atom in quantum optics experiments. Having such an 'artificial atom' will greatly improve flexibility and preciseness in experiments, thereby enhancing the discovery of new physics. This is because we will no longer be constrained by what natural can provide. Rather, one will be able to tailor transition energies and optical matrix elements to enhance the physics of interest.

2. Approach

Much of our modeling and experiments were based on variations of a 4-level QC scheme. In the case of 4-wave mixing (Fig. 1), the combination of drive field absorption and emission (waves 1 and 2) together with probe field absorption (wave 3) modifies the polarization (wave 4) connecting levels 1 and 2. In our scheme, this polarization provides THz gain with phase matching automatically satisfied. The simulations also revealed a quantum coherence contribution arising from the polarization between the optically forbidden transition connecting levels 1 and 3 (see Fig 2). This polarization is created by the interference of probe and drive fields. Owing to the quantum coherence, THz gain is achieved for drive intensity below that need for creating a population inversion. Without a population inversion, device efficiency improves because of decreased sensitivity to nonradiative carrier losses.

As may be seen in Fig. 3, the 4-level QC configuration incorporates the basic properties of 4-wave mixing and quantum coherence. Furthermore, it contains features that are not obtainable with atomic systems. We summarize them below.

1) Separate transitions for absorption and emission of drive field, which is important for the present goal of THz generation with drive field recovery, and for the future goal of producing entangled photons.

2) Forward electric bias to shoe-horn in the THz transition (levels 2 and 3) and to provide power for the THz radiation.

3) Spatial variation in doping, so that the electron population in the lowest energy level (4) is actually smaller than that in the higher lying level 1, thereby creating a Raman inversion.

4) Possibility of tailoring level energies and dipole matrix elements during quantum well growth to maximize 4-wave mixing and quantum coherence processes.

5) Cascading (not shown in Fig. 3) to drain the electron population in level 4 and to generate more THz photons.

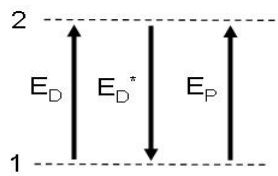

Fig. 1. 4-wave mixing

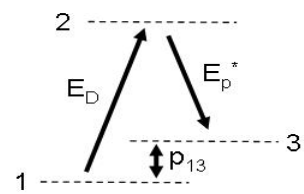

Fig. 2. Quantum coherence

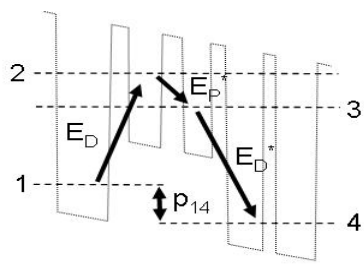

Fig. 3. 4 - level QC structure

The above features combine to make possible the generation of coherent THz radiation, with no depletion of drive photons (hence, no Manley Rowe limitation). Energy is conserved by deriving the energy for the THz photon from the electrical bias.

3. Results

Experiments

FTIR and photoconductivity measurements were made for an intersubband photo-current multiplier. Also measured was the photoconductivity of a digital superlattice OPED sample. Details are given in Appendices I, II and III. The design of the experimental structures involved detailed modeling of bandstructure and carrier collision effects. Details of the model and code developed and used in the investigations are published in a journal article [1].

Theory

During characterization of laser structures, we discovered interesting dynamical behaviors that are possibly related to coherence collapse. That such enhanced dynamical nonlinearities occur in quantum cascade lasers is not well understood. There are practical implications in terms of frequency stability and modulation response. Also, there is scientific interest in terms of dynamical instabilities in a new class of lasers. Furthermore, there is potential application for detecting a weak laser signals from a remote source in the presence of strong background noise (TA 11349). Details are discussed in three papers [2-4].

Work was performed on solving of the optical Bloch equations for a multilevel system interacting with a quantized radiation field. The equations described a fully quantized (i.e.,

quantized active medium and quantized radiation field) light-matter system operating in the strong-coupling (polariton) limit. Results to date are described in 2 publications [5-6]. The system has applications in brightness enhancement (TA 11318), quantum nondemolition and ultra-small (subwavelength) volume lasers.

Invention Disclosures

Several TAs were produced involving the use of intersubband and intersubband/interband structures to modify radiation properties. These disclosures are described in Appendices D.

References

[1] In`es Waldmueller, Michael C. Wanke, Maytee Lerttamrab, Dan G. Allen, and Weng W. Chow, ' Inverse-Quantum-Engineering: A New Methodology for Designing Quantum Cascade Lasers,' IEEE J. Quantum Electron. **46**, 1414, 2010.

[2] W. W. Chow and S. Wieczorek, ‘Using chaos for remote sensing of laser radiation,’ Optics Express **17**, 7491-7504, 2009.

[3] S. Wieczorek and W. W. Chow, ‘Bifurcations and chaos in a semiconductor laser with coherent or noisy optical injection,’ Optics Commun. **282**, 2367, 2009.

[4] D. G. Allen, T. W. Hargett, J. L. Reno and M. C. Wanke , 'Optical bistability from domain formation in terahertz quantum cascade lasers,' (to be published in IEEE J. Selected Topics in Quantum Electron.)

[4] A. Carmele, M. Richter, W. W. Chow and A. Knorr, ‘Antibunching of thermal radiation by a room-temperature phonon bath: a numerially solvable model for a strongly interacting light-matter-reservoir system,' Phys. Rev. Lett. **104**, 156801, 2010.

[5] J. Kabuss, Alexander Carmele, M. Richter, W. W. Chow and A. Knorr, 'Inductive equation of motion approach for a semiconductor QD-QED: coherence induced control of photon statistics,' (accepted physica status solidi).

Appendix A: FTIR measurements of V121049 (DASPMT02a) wide barrier photo-current multiplier

1 Sample

Sample is design DASPMT02a (see report in Wavefunction Programs/Structures), grown by MOCVD by Greg Peake at 3.33 Å/sec, which is 1/3 of his usual growth rate of 10 Å/sec. Many active region periods are include for spectroscopy. Samples are fabricated according to the layout in Fig. 3 and growth request (Fig. 2. A "plasmon test" mask sample was co-processed (V121049T) for photocurrent measurements.

Prior to mounting on a copper submount the sides of the bottom contact are cleaved to leave only 1 mm of bottom contact on either side (10 mm total width) to fit between the screws on the sample mount. Top metal is PdGeTiPtAu (750/1350/300/500/1000 Å). Ni was deposited in-situ as an etch mask (2000 Å). The ICP etch recipe (GaICP tool) is X-GaAs Etch 25W_750W. The etch rate is comparable to the standard GaAs etch, but less bombardment occurs (higher selectivity for Ni). Ni is removed using Transene TFG Ni etchant at 50 C for 2 minutes. The bottom contact is GeAuNiAu, annealed to 400 C for 30 seconds. Sample was lapped and polished to 280 μm thickness. Backside Ti/Au (200/2000 Å) was deposited. Then the sample was cleaved into 4 mm and 2mm bars for facet polishing using a 45° jig, 600 grit sand paper, 3 μm Fibremet polish film (nonadhesive), and Chemlox on a piece of polish pad, 2 minutes each, with a thorough rinsing and glove exchange between steps. The sample is held to a glass slide with crystal bond and the facet and front surface are also protected by melting crystalbond over the samples before polishing.

The 4 mm sample was mounted and measured, but deemed to be too absorptive, so the 2 mm sample with 1.5 mm face area was used for most of the measurements.

4 bond pads are epoxied to the standard mount and a quad pin socket is soldered to the bond pads. The sample was glued to the mount with GE Varnish (not recommend, used for expedience. Use In melt bonding for most cases), wire bonded (taking care to curl the wire bonds to the mesa out of the optical path), and screwed to the Al 45/45 sample mount for the Cryo Industries cryostat.

1.1 Measurement setup

The cryo-industries cryostat was used for measurements. It was clamped using 0.5" pedestal posts to a kinematic plate. The locators for the plate are plungers that are depressed under the weight of the cryostat so 1/4 screws with nuts have to be used to fix the height. (Use $CaFl_2$ beamsplitter and NIR source to align to sample w/o windows.) See Fig. 4. Black tape and black Al foil are used to shield stray transmission. KBr windows were used for the cryostat, making 4 KBr windows total, including the two KBr windows for the Bruker sample compartment. (Remove sample kinematic plate, evacuate Bruker, vent sample chamber, replace kinematic plate and shield.) Nitrogen purge was used along with open containers of Drierite desiccant to reduce H_2O vapor absorption.

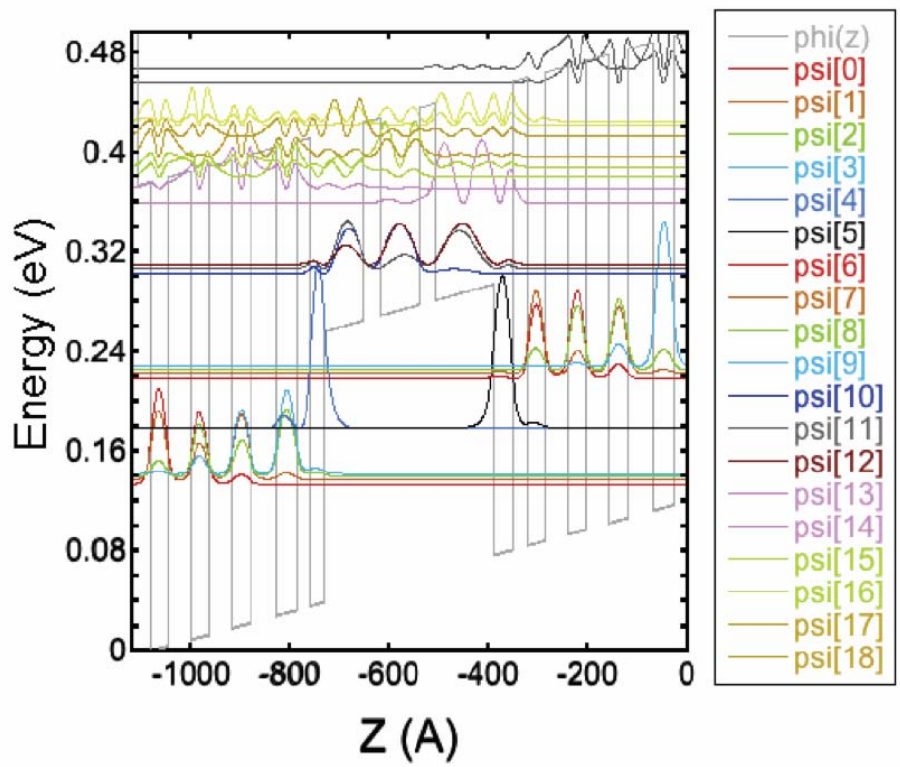

Figure 1: Wavefunctions for design DASPMT02a at 11.1 kV/cm bias. States of interest are the pump state ("ψ_5", black), excited miniband states (ψ_{10}–ψ_{12}, blue, grey, burgundy), recycle state (ψ_4, sky), and extractor state (ψ_3, turquoise). Transitions are $E_{4,5-10}$=124 meV, $E_{4,5-11}$=128 meV, $E_{4,5-12}$=-132 meV, E_{6-5}=-40 meV, E_{4-3}=36 meV. Dipoles are $|z|_{5-10/11/12}$=1.6/4.7/ 5.2 Å; $|z|_{5-10/11/12}$=7.4/7.6/4.8 Å; $|z|_{12-11}$=87 Å; $|z|_{11-10}$=67 Å.

GaAs	0	1000	4.00E+18	1
AlGaAs	0.45	27	0	35
GaAs	0	41	0	35
AlGaAs	0.45	51	0	35
GaAs	0	39	0	35
AlGaAs	0.45	46	0	35
GaAs	0	37	0	35
AlGaAs	0.45	46	0	35
GaAs	0	35	1.00E+17	35
AlGaAs	0.45	29	0	35
GaAs	0	40.5	1.00E+17	35
AlGaAs	0.24	116	0	35
AlGaAs	0.45	31	0	35
AlGaAs	0.24	79	0	35
AlGaAs	0.45	35	0	35
AlGaAs	0.24	79	0	35
GaAs	0	29	0	35
AlGaAs	0.45	27	0	35
GaAs	0	41	0	1
AlGaAs	0.45	51	0	1
GaAs	0	39	0	1
AlGaAs	0.45	46	0	1
GaAs	0	37	0	1
AlGaAs	0.45	46	0	1
GaAs	0	10000	4.00E+18	1
AlGaAs	0.45	450	0.00E+00	1
GaAs	0	440	0.00E+00	1
AlGaAs	0.45	450	0.00E+00	1
GaAs substrate (SEMI-INSULATING)				

Figure 2: Growth request. Columns are Al fraction, thickness (Å), doping, and number of repeats (periodic, not collated).

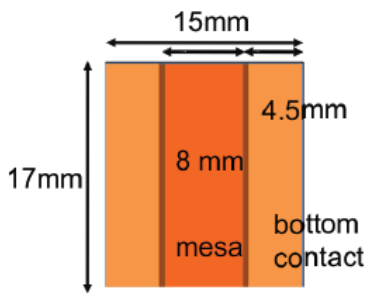

Figure 3: Layout for V121049M. Lateral (bottom) contact spacing from mesa is 30 μm.

1.2 Bruker settings

- Bruker hardware: For rapid scan measurements the Globar MIR source was used with a 5 mm aperture, KBr beamsplitter aligned under vacuum to DTGS detector (3mm aperture during align), KBr sample chamber windows, For step scan the aperture was 6 mm.
- Detector: MCT detector D316 (red) for rapid scan or MCT DC out for step scan, liquid N_2 cooled. For DC out connect DC out cable to "MCT DC out port" feedthru. To select detector for step scan a careful procedure must be followed to trick the Bruker. Select "Bolometer" and then "check signal" with all experimental parameters as desired. Exit experiment window. Open direct command entry window. Type "DTC=2" and hit enter. Exit window. Open "Step scan modulation" window choose parameters without changing the optics settings or looking at "check signal". Perform the scan. This moves the mirror but does not change which port the ADC measures. Be sure to select the ADC board coupling switch on the side of the Bruker to "DC coupling".
- Measurement parameters: Scans were taken at various sample voltage and temperatures with data taken from 500 cm^{-1} to 8000 or 6000 cm^{-1}. Scan resolution was 5 cm^{-1}, then 3.5 cm-1 for rapid scan, The Mertz unsigned algorithm was used for the Fourier transform with 2 bit zerofilling. For the higher resolution data 100 or scans were averaged. For the voltage dependence at lower temperatures 1500 scans were averaged. The scanner HeNe fringe rate was 80 kHz. Higher res data was single sided rapid return. Lower res voltage dependence data was double sided forward backward scanning.

2 data

Absorption measurement data is stored in folder IPM-abs. I-V data is stored in the other folders.

2.1 I-V curves

Fig. 5a show current vs. voltage/electric field, and differential resistance dV/dI, normalized to device area (5 x 1.5 mm). Fig. 5b shows I-V curves versus sample temperature. The sample wasn't

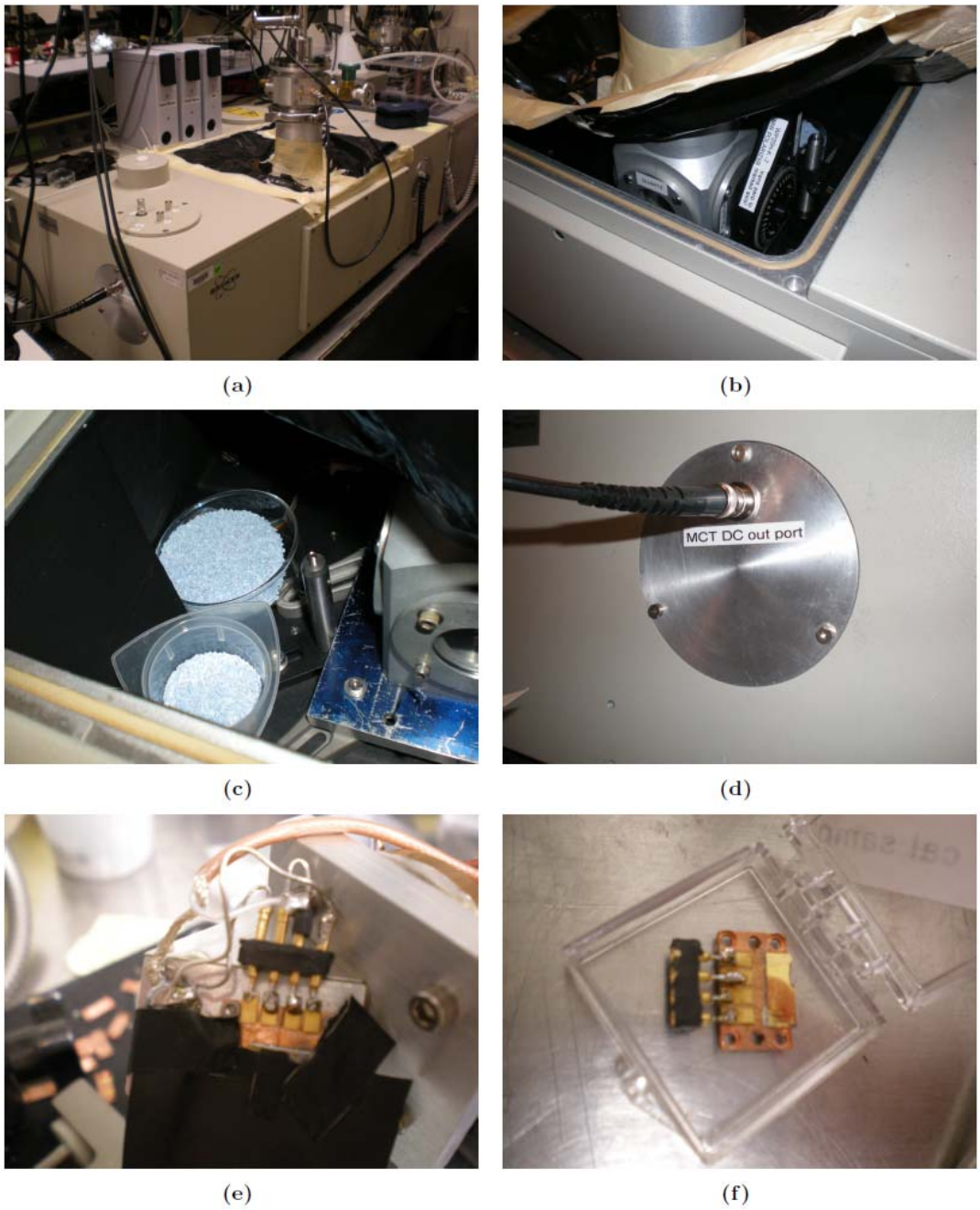

Figure 4: (a) Bruker with black plastic enclosure, N_2 purge line (behind cryostat), and Cryo Industries cryostat (b) front window with motorized polarizer rotator holding KRS-5 polarizer, in a CVI kinematic post mount (use Thorlabs APT software), (c) open jars of desiccant, pedestal clamps and locator stop (d) DC output of MCT feedthru (e) sample wired up in 45/45 mount with black anodized Al foil (blackwrap) and black Anodized Al foil tape (blacktak) (f) typical thick FTIR sample on a wide sample mount. Thinner samples can be mounted on the regular quad hole mounts as in (e).

heat sinked properly, so I didn't take it up to room temperature. Three points are worth noting. The total current is at least three orders of magnitude higher than expected, and only 4-8 times better than the OPED sample, despite a barrier that is much wider. However, no NDR is observed. Ostensibly the current could be reduced by going lowering the temperature even more. Also, no thermal runaway is observed at the lower 11 kV/cm design bias. At higher biases equivalent to the OPED sample (17.5 kV/cm), a very strong current turn-on was observed. Note this sample was not heat sinked very well, and the device area is quite large.

This suggests that all the OPED samples will have thermal runaway issues if the design bias is high. The digital superlattice samples VB0349, VB0350 are designed to operate above 20 kV/cm.

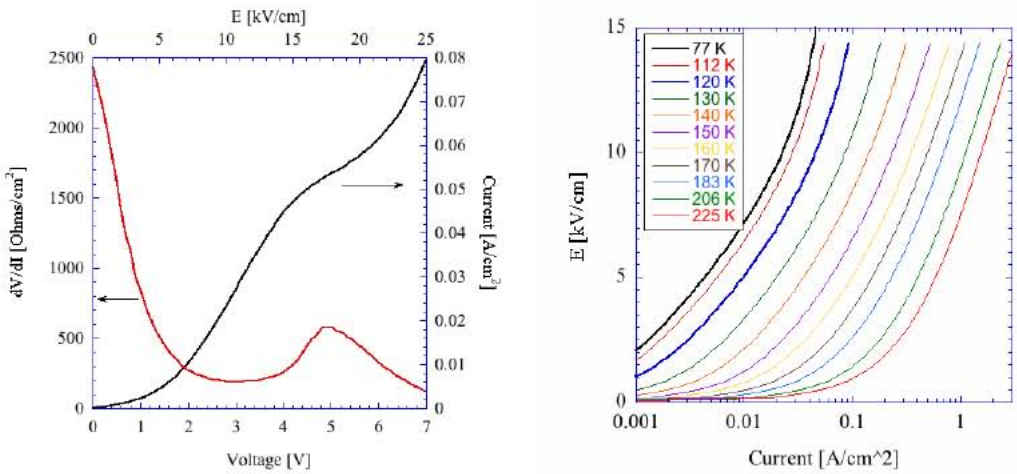

(a) (b)

Figure 5: (a) Current-voltage curve with electric field axis for reference. Also left derivative dV/dI versus voltage/electric field. Minimum of dV/dI is 3.1 V, or 11.15 kV/cm^2. (b) Log-linear plot of current versus applied electric field for a series of temperatures.

2.2 MIR absorption

Spectra were taken with and without the system under vacuum (sample chamber vented when under vacuum), with and without cryostat windows, without a polarizer and with a polarizer in TM and TE polarization. TM polarization corresponds to the electric field parallel to the growth direction. The sample was aligned to normal incidence on the 45° facet so that the back reflection from the facet retraced the incident beam (I did this with the $CaFl_2$ beamsplitter and NIR source).

Bruker software/hardware bug: If the signal drops by a lot after venting to vacuum and then repumping or changing beamsplitters and changing back or something like that, then try adjusting the scanner speed to some other value. That will fix the bug, whatever it is. Then you can change the speed to the desired value.

Only a few scans were taken for the 4.5 mm thick sample. The transmission for the TM polarization was much lower than for the TE, about five times lower total intensity) and there

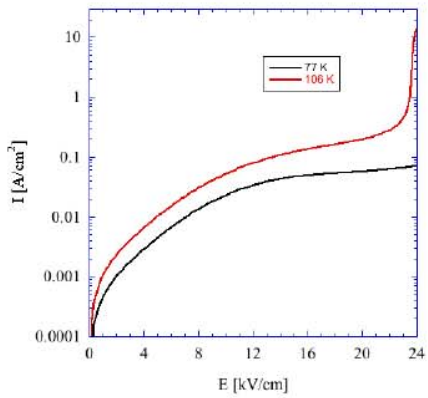

Figure 6: I-V curves at higher bias showing thermal runaway for currents exceeding 0.2 A/cm^2 at biases above 22 V.

was almost no transmission at certain frequencies, which means the line shapes are distorted and broadened. Based on the TM/TE ration, there are three absorption regions, one near 900 cm^{-1} (very strong), one near 1400 cm^{-1}, and one a little further than that. The ratioed spectra show ringing in the high frequency components despite a deliberate wedge of at least five degrees in the parallelism of the facet planes (polished sample looks like trapezoid from top instead of rectangle). The height was set by adjusting the locating feet on the kinematic plate, with the NIR source and $CaFl_2$ beamsplitter by looking at the focal spot on the sample. The horizontal alignment was also done by inspection by sliding the cryostat and clamping it in position. The position was optimized by moving the cryostat forward and backward while illuminating with the Globar source, with the DTGS detector. The transmission doesn't go all the way to zero, which may be a polarization misalignment or background from a light leak around the sample, or partial reflection/substrate guiding from the buried contact layer. Also there was an iffy connection somwhere and I coudn't get reliable I-V data.

So I switched to a 1.5 mm long sample (2 mm pre-polish). The transmission was higher but the 900 cm^{-1} feature was still very deep. The TE transmission was on the order of 1.6 times larger than TM. With this sample I took TE and TM data at a variety of temperatures, and looked at bias ratioed spectra and temperature ratioed spectra and two different biases. However, peak position shifts were not easy to detect in the his way.

Instead, I measured dithered the bias and locked in to the change in sample transmission with bias. The procedure was as follows:

1. Detector setup: Break black plastic atmospheric seal, stop purge, remove desiccants, remove kinematic plate containing the cryostat and polarizer . Evacuate sample chamber. Vent optics. Remove bolometer from bolometer port. Attach "MCT DC out" feedthru port to Bruker and connect the DC out from the MCT to the feedthru. Replace covers. Evacuate Bruker. Vent sample chamber. Replace cryostat and desiccant, seal chamber with black plastic and purge. Evacuate cryostat and cool sample by pouring liquid nitrogen into the

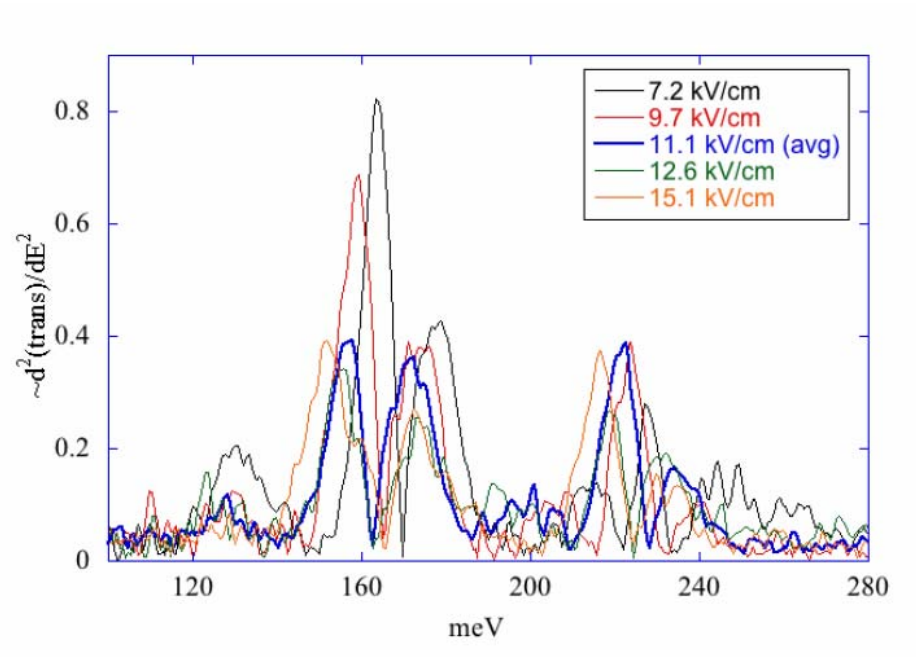

Figure 7: (a) Transmission change with change in applied bias (0.6 V_{pp}) for various offset voltages/electric fields. Transitions observed at 130, 160, and 230 meV are assigned in Fig. 8. The data for the 11.1 kV/cm bias was the average to two scans, one at 572 Hz dithering frequency, and one at 1032 kHz, to improve the SNR. The 15.1 kV/cm sample is the average of two 572 Hz spectra.

cold finger chamber with a funnel.

2. Electronics setup: Connect a function generator to the sample. Set frequency to >500 Hz. Set AC square wave voltage to 0.6 V. Offset will be varied for the experiments. Connect trigger out to lockin reference in. Connect MCT DC out to lockin input. Connect lockin output to Bruker external input ("bolometer") port. Auto phase with 0.6 V applied. Select X output. Time constant was varied. 100 ms was sufficient to collect data.

3. Bruker settings: Open experiment window, select MCT detector. Ensure all other optics parameters are correct. Check signal. Exit experiment window. Open direct command entry window. Type DTC=2. Enter. Close window. Open step scan modulation window. Select 10 co-additions, 300 ms stabilization delay, and data window 600 cm^{-1} to 2500 cm^{-1}.

The resulting signal (Fig. 7) is a mixture of the first derivative of the transmission with respect to the applied voltage and the second derivative. The signal looks like the absolute value of a first derivate or else a second derivative. This may have to do with the phase I picked for the lockin (auto-phase at zero volts offset).

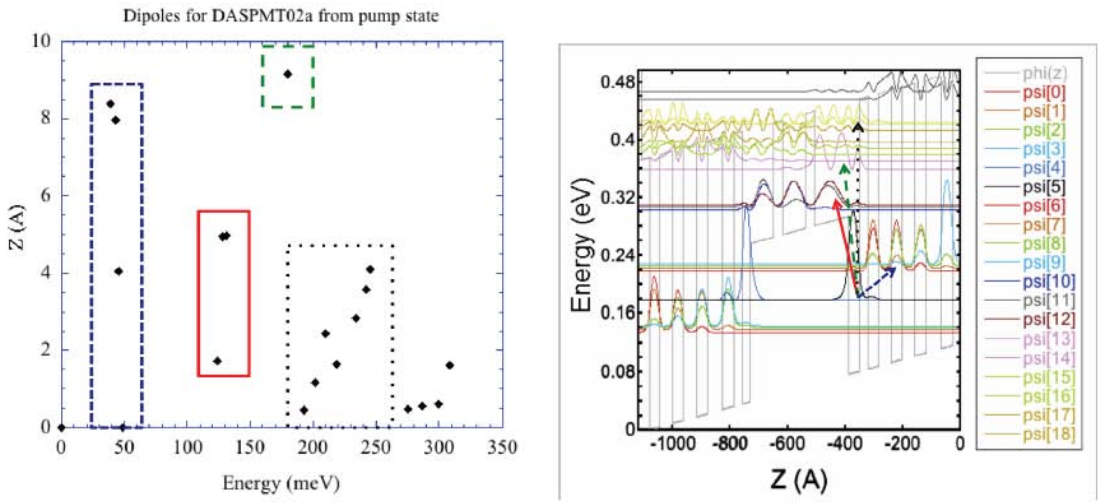

(a) (b)

Figure 8: (a) Calculated transition energies from occupied pump state level with boxes corresponding to labels for transitions shown in band diagram (b). Blue: pump state to injector miniband; red: pump state to barrier miniband; green: pump state to next excited state above barrier miniband; black: pump state to various excited barrier states. Comparison of theory and measurements is in table. Response at frequencies lower than the pump to elevated miniband transitions is likely due to excitation out of the less populated injector miniband.2.2.

Initial state	Upper state	Calc (meV)	Meas	Comment
5 (pump)	6–9 (injector)	39–48	n/a	KBr opaque; beyond det. range
5 (pump)	10–12 (barrier)	123–131	130	agreement
5 (pump)	13 (next exc. state)	180	160	expt. $<$ calc
5 (pump)	15–16 (exc. states)	200-210	190–210	good agreement
5 (pump)	17–20 (exc. states)	234–245	220–240	good agreement

2.3 Missing data

Low temperature I-V: measure tunnel current XRD: get Al ratios and growth rate Linear photocurrent spectroscpy vs. bias: observe difference between alignment bias and maximum photocurrent bias. Nonlinear photocurrent spectroscopy vs. sample width: compare on and off resonance to observe recycling

3 Conclusions

Good agreement between experiment and theory is achieved for the alignment bias (11.1 kV/cm) and pump transition energy (125-130 meV). Poorer agreement is achieved for the transitions to the next excited state, which is supposedly well localized. A more delocalized wavefunction may be lower in energy, due to perhaps the finite interface broadening. I have not yet received XRD for this sample to verify Al ratios and growth rate, however the etch depth through the buried reflector is 1.04±0.03. times the expected rate, which is very good for this as-yet unoptimized MOCVD growth. The higher than expected current is likely due to thermal excitation and the higher doping of the sample.

Future samples should be grown with 10, 3 and 1 active region, for photocurrent spectroscopy. High Q cavities should be used to improve radiative recycling efficiency. Lower doping may be used to limit current, at the expense of absorption. An optimal design may have the absorption Q match the bare cavity Q (absorption time=cavity life time). So lower doping could be used with a higher Q cavity, to improve the recycling rate at constant absorption, since the recycling rate depends on the intensity in the cavity (Q) and mode overlap with the active region.

Current should be measured at 4 K, to see exactly where the tunnel-lock voltage is. However, the largest uncertainty in that measurement is the contact resistance voltage drop. I assumed zero for this case, because the currents were fairly low and the doping of the contact layers was quite high.

Electrically-detected FTIR may be possible by monitoring the sample photocurrent under bias if the sample is cooled sufficiently, to where the tunnel current equals the thermal current. This provides linear photoresponse. An SRS current preamplifier is needed for this measurement and optical chopping. Otherwise the CO_2 laser will have to be used for photocurrent spectroscopy. The CO_2 laser will have to be used in any case for the nonlinear photoresponse. The good news is the sample appears to have absorption in the upper branch of the CO_2 laser range.

Appendix B: Photoconductivity of VB0349 (Digital superlattice OPED)

1 Sample

Sample is design DASOPED05i (Fig. 1a, see report in Wavefunction Programs/Structures), grown by MBE by Terry Hargett. A "plasmon test" mask sample was used for photocurrent measurements, with the superlattice exposed by cleaving down the center of the waveguide and mounting the sample side-on to the CO_2 illumination. Side facets are also cleaved in anticipation of THz lasing. This sample was mounted facing on the wrong side of the C-mount and any THz emission would go into the CO_2 laser containment box.

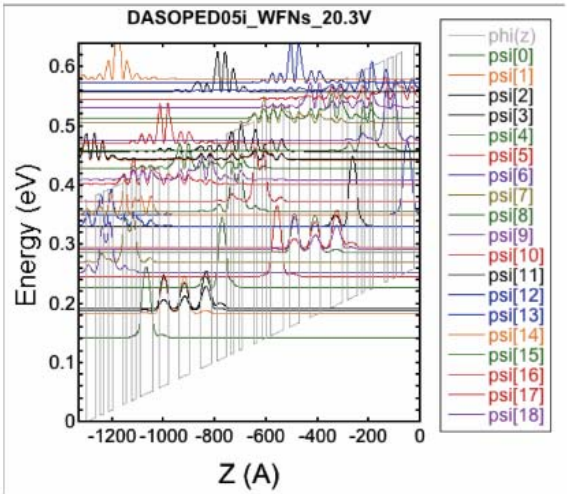

(a)

1.5 Layer structure for growth

Layer	Material	Al fraction	Thickness (Å)	Comment
1	GaAs		800	5e18 Si
2	AlGaAs	0.45	39.6	undoped
3	GaAs		42.5	"
4	AlGaAs	0.45	39.6	"
5	GaAs		38	"
6	AlGaAs	0.45	26	undoped, end SL]
7	GaAs		46.5	doped 1.5e17 (Si)
8	AlGaAs	0.45	19.8	undoped
9	GaAs		14.1	"
10	AlGaAs	0.45	19.8	"
11	GaAs		14.1	"
12	AlGaAs	0.45	42.4	"
13	GaAs		14.1	"
14	AlGaAs	0.45	19.8	"
15	GaAs		14.1	"
16	AlGaAs	0.45	14.1	"
17	GaAs		38.5	"
18	AlGaAs	0.45	19.8	"
19	GaAs		46	"
20	AlGaAs	0.45	39.6	"
21	GaAs		42.5	"
22	AlGaAs	0.45	39.6	undoped
23	GaAs		38	doped 1.5e17 (Si), begin SL (150 repeats)]
24	GaAs		2500	5e18 Si
25	GaAs		2000	2e18 Si
26	GaAs		2000	8e17 Si
27	AlGaAs	0.55	2500	Etch stop
28	GaAs		3000	undoped Buffer w/pauses
	Total		8.475 μm	total epilayer thickness
	Substrate		~650 μm	SI-GaAs

(b)

Figure 1: (a) Wavefunctions for design DASOPED05i at 20.1 kV/cm bias. Transitions are E_{5-16}=127 meV (9.76 μm), E_{4-15}=127 meV, $E_{4,15-5,16}$=18 meV. Dipoles are $|z|_{5-15/16}$=2/8 Å; $|z|_{4-15/16}$=12.2/4.7 Å; $|z|_{16-15}$=29 Å.

1.1 Measurement setup

A sample (VB0349pIb20B-L) was cleaved along the ridge with 1 mm length and 200 mum width active region. Sample was mounted to expose lateral cleaved edge of laser ridge to incident CO_2 laser excitation. Sample was In-melt bonded to a C-mount and screwed to the side of a rectangular copper cold finger with In foil in between for a good connection to the heat sink. The C-mount was contacted by clips, with the laser mesa grounded and positive voltage applied to the lateral contact. The cryo-industries cryostat was mounted on pedestal pillars inside the plexiglass-protected, interlocked CO_2 photoconductivity setup. The cryo-industries cryostat was clamped using pedestal posts to to the optical table inside the laser enclosure. The plexiglass box was closed and open containers of Drierite desiccant were used to reduce fogging of the KBr windows. (Suggestion: look into getting ZnSe windows.) The low power path is used with a 1 cm diameter beam with total power after the Brewster polarizer of 200 mW and maximum estimated intensity incident on the sample of 10 W/cm^2 and incident power on the superlattice region was less than 1.5 mW (active region is 7.7 μm thick and 2 mm long).

THe excitation light from the tunable CO_2 laser was modulated with a 30 slot chopper at 1.8 kHz. Sample bias was provided by an HPE3611A DC supply and measured by the SR570 current preamplifier. 10^4 V/A gain was used with the low noise setting. SR570 high and low pass filter frequencies were set to 300 Hz and 10 kHz. -200 muA current offset was used to keep signals close to zero. Signal was detected by the EG&G 5209 single phase analog lockin amplifier. No line of band pass filters were needed. Autophase was done at a point of maximum positive photocurrent, and the in-phase current response was recorded. Sensitivity scale was optimal at 30 mV, depending on wavelength and intensity used and the time constant was 300 ms, though 100 ms was sufficient for two and a half digit certainty. No change in signal amplitude was observed versus chopping speed suggesting LC response is not an issue at these low chopping frequencies.

2 Data

See 091218_PMT_photoconductivity_report for schematic of experimental setup. For I-V response, the sample showed avalanche behavior at a bias of 19.5 V (25.3 kV/cm) at 202 K. The sample avalanched at the design bias (15.5 V, or 20.3 kV/cm) at 220 K. The superlattice showed NDR below 140 K at the pump/recycle crossing ($\sim$ 11 kV/cm). At very low temperatures below 40 K another NDR showed at 1 V bias, which broke at a 6 V bias.

Photoconductivity data (Fig. 3) at 200 mW incident intensity ($\sim$ 9 W/cm^2) shows photoconductivity rising with bias at all wavelengths. A photocurrent peak shifts to higher bias with increasing wavelength. The longest wavelengths show no peak, but monotonic response versus bias. The peak occurs at the design bias of 20.3 V for 9.35μm excitation (133 meV). This is very nearly the design transition energy for the structure of 127 meV. The high photocurrent obtained for the shortest wavelength scan appears to be anomalous, but may be related to ionization out of the upper laser state. The high photocurrent observed for the 9.45 mum excitation may be due to cross pumping from the pump state to the recycle state, since that transition energy

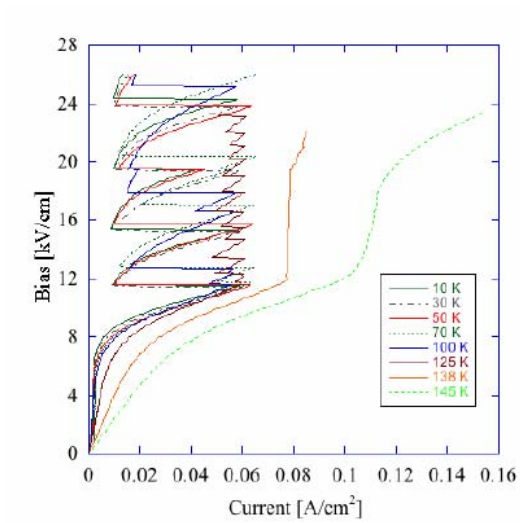

Figure 2: I-V of VB0349pIb20B-L at various temperatures.

Photocurrent responsivities were measured in the linear range, verified by an approximately linear power dependence.

3 Conclusions

Good agreement between experiment and theory is achieved for the alignment bias (11.1 kV/cm) and pump transition energy (125-130 meV), which is consistent with FTIR absorption measurements. Linear photoresponse of 7×10^{-3} electrons/photon was achieved.

Plans: proceed with low duty cycle ($\sim \mu$s chopped pulse) high power photobleaching/optically pumped transparency measurement. Grow new samples with fewer layers for less loss and incorporation into a large mode area, low loss cavity, to increase the electric field per photon and observe onset of transparency/latching at lower intensities. Check photocurrent vs. power on/off resonance for several sample depths (200, 100, 50 μm) to observe photo-induced transparency.

Appendix C

Photoconductivity measurements of a wide barrier photo-current multiplier

1 Sample

Sample is design DASPMT02a (Fig. 1a, see report in Wavefunction Programs/Structures), grown by MOCVD by Greg Peake at 3.33 Å/sec, which is 1/3 of his usual growth rate of 10 Å/sec. Many active region periods are include for spectroscopy (Fig. 1b). A "plasmon test" mask sample (V121049T) was used for photocurrent measurements.

1.1 Measurement setup

A sample was cleaved along the ridge with 1 mm length and 200 mum width active region. Sample was mounted to expose lateral cleaved edge of laser ridge to incident CO_2 laser excitation. Sample was In-melt bonded to a C-mount and screwed to the side of a rectangular copper cold finger with In foil in between for a good connection to the heat sink. The C-mount was contacted by clips, with the laser mesa grounded and positive voltage applied to the lateral contact. The cryo-industries cryostat was mounted on pedestal pillars inside the plexiglass-protected, interlocked CO_2 photoconductivity setup. The cryo-industries cryostat was clamped using pedestal posts to to the optical table inside the laser enclosure. The plexiglass box was closed and open containers of Drierite desiccant were used to reduce fogging of the KBr windows. (Suggestion: look into getting ZnSe windows.) The low power path is used with a 1 cm diameter beam with total power at PM (Fig. 2) of 200 mW and maximum estimated intensity incident on the sample of 10 W/cm^2 and total absorbed power less than 3 μW (active region is very narrrow).

THe excitation light from the tunable CO_2 laser was modulated with a 30 slot chopper at 1.8 kHz. Sample bias was provided by internal battery of SR570 current preamplifier and measured by a voltmeter. 10^6 V/A gain was used with the low noise setting. SR570 high and low pass filter frequencies were set to 100 Hz and 10 kHz. No current offset was needed. Signal was detected by the EG&G 5209 single phase analog lockin amplifier. No line of band pass filters were needed. Autophase was done at a point of maximum positive photocurrent, and the in-phase current response was recorded. Sensitivity scale ranged from 10mV to 1V, depending on wavelength and intensity used.

2 Data

Photoconductivity data (Fig. 3) at 200 mW incident intensity ($\sim$ 9 W/cm^2) shows photoconductivity rising with bias at all wavelengths, and higher total response at long wavelengths, where the peak absorption occurs at higher bias, for which the tunnel barrier is least effective. A peak in the photoresponse vs. bias is observed at all wavelengths. The peak with minimum width occurs at 11.2 kV/cm bias (3.1 V bias), for 9.7 μm (128 meV) radiation. This is very nearly the design bias and transition energy for the structure.

The peak photocurrent bias was observed to shift to lower biases with increasing intensity in the range 1–10 W/cm^2 at all wavelengths, by approximately -0.15$\pm$0.05 V (-0.5$\pm$0.02 kV/cm).

Photocurrent responsivities were measured in the linear range, verified by an approximately linear power dependence.

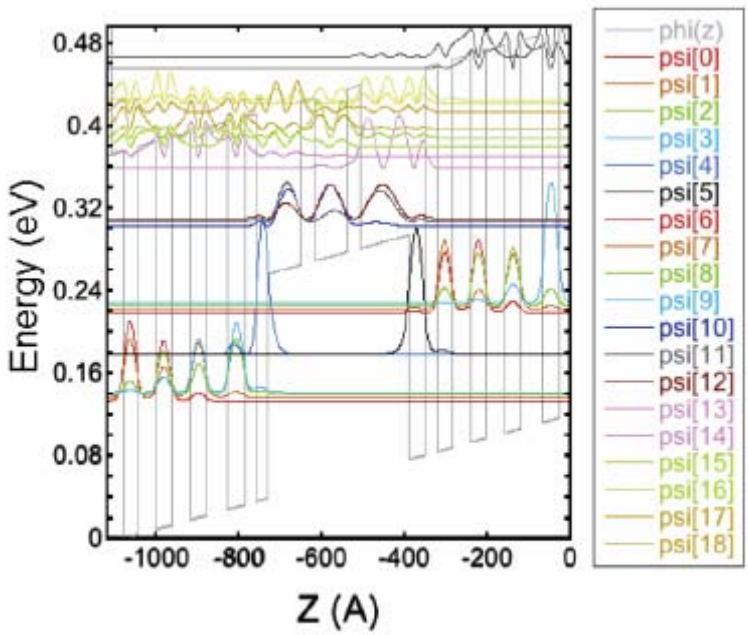

(a)

GaAs	0	1000	4.00E+18	1
AlGaAs	0.45	27	0	35
GaAs	0	41	0	35
AlGaAs	0.45	51	0	35
GaAs	0	39	0	35
AlGaAs	0.45	46	0	35
GaAs	0	37	0	35
AlGaAs	0.45	46	0	35
GaAs	0	35	1.00E+17	35
AlGaAs	0.45	29	0	35
GaAs	0	40.5	1.00E+17	35
AlGaAs	0.24	116	0	35
AlGaAs	0.45	31	0	35
AlGaAs	0.24	79	0	35
AlGaAs	0.45	35	0	35
AlGaAs	0.24	79	0	35
GaAs	0	29	0	35
AlGaAs	0.45	27	0	35
GaAs	0	41	0	1
AlGaAs	0.45	51	0	1
GaAs	0	39	0	1
AlGaAs	0.45	46	0	1
GaAs	0	37	0	1
AlGaAs	0.45	46	0	1
GaAs	0	10000	4.00E+18	1
AlGaAs	0.45	450	0.00E+00	1
GaAs	0	440	0.00E+00	1
AlGaAs	0.45	450	0.00E+00	1
GaAs substrate (SEMI-INSULATING)				

(b)

Figure 1: (a) Wavefunctions for design DASPMT02a at 11.1 kV/cm bias. States of interest are the pump state ("ψ_5", black), excited miniband states (ψ_{10}–ψ_{12}, blue, grey, burgundy), recycle state (ψ_4, sky), and extractor state (ψ_3, turquoise). Transitions are $E_{4,5-10}$=124 meV, $E_{4,5-11}$=128 meV, $E_{4,5-12}$=-132 meV, E_{6-5}=-40 meV, E_{4-3}=36 meV. Dipoles are $|z|_{5-10/11/12}$=1.6/4.7/ 5.2 Å; $|z|_{5-10/11/12}$=7.4/7.6/4.8 Å; $|z|_{12-11}$=87 Å; $|z|_{11-10}$=67 Å. (b) Growth request. Columns are Al fraction, thickness (Å), doping, and number of repeats (periodic, not collated).

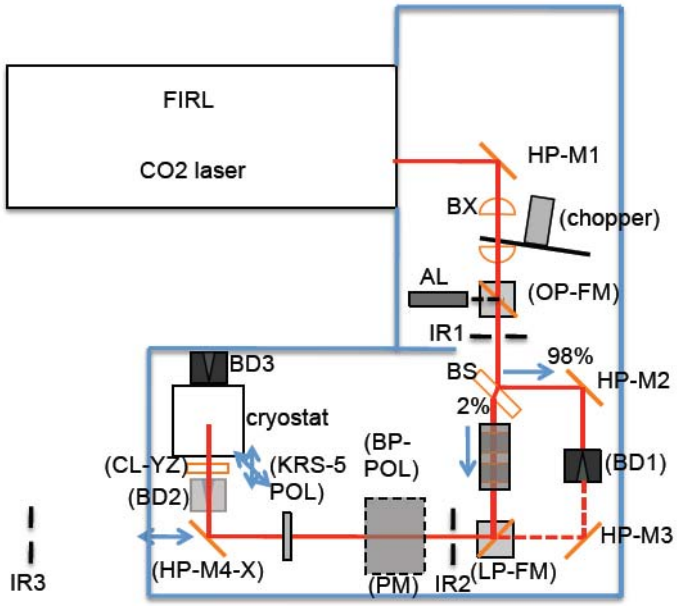

Figure 2: Diagram of photoconductivity setup with removable elements in parentheses. Emission from CO_2 port of FIRL reflects from high power mirror 1 (HP-M1), a three screw kinematic mount on a sliding guide for horizontal position and gimballed anglular positioning of the beam. The beam passes through a 1:1 beam expander (BX) setup which focuses the light down to a small area so that a 30 slot chopper blade can be used to modulate the beam and allows to compensate for the slight divergence in the beam by adjusting the axial position of the second lens. The visible alignment laser (AL) is optionally inserted via a flip mount with an optical mirror (OP-FM) prior to the first iris (IR1)–*block CO_2 at source prior to flipping mirror.* A ZnSe plate beam splitter (BS) reflects 98% of the S-polarized (vertically polarized) 10 μm light. The reflection may be collected with a beam dump (DB1), or brought to the sample via high power mirrors HP-M2 and HP-M3. *Remove KRS-5 polarizer (KRS-5 POL) and power meter (PM) before admitting the high power beam.* The BS transmission passes through the optional Brewster plate polarizer (BP-POL), reflects at low power mirror on a flip mount (LP-FM) and passes through the second iris (IR2). The Scientech power meter (PM) may be inserted on a kinematic base if the power is less than 10W. Similarly, the KRS-5 thin film wire grid polarizer (KRS-5 POL) may be used with the low power beam as an analyzer. For power dependence studies BP-POL may be rotated. If using BP-POL with the high power path, the exit port must be opened and dumped. A high power analyzer, such as another Brewster plate, is needed for use as an analyzer, with additional beam dump. The beam is directed to the sample with HP-M4-X, a high power mirror on an X translation stage. Optionally, a beam dump (BD2) may be inserted after HP-M4-X. When adjusting the alignment of the visible laser on IR3 (outside the enclosure) with OP-FM, the HP-M4-X post maybe removed (kinematic post collar). A f=50 mm cylindrical lens (CL-YZ) on a rotation mount and YZ stage focuses the light in the vertical direction to a horizontal line focus at the sample, followed by a safety beam dump (BD3).

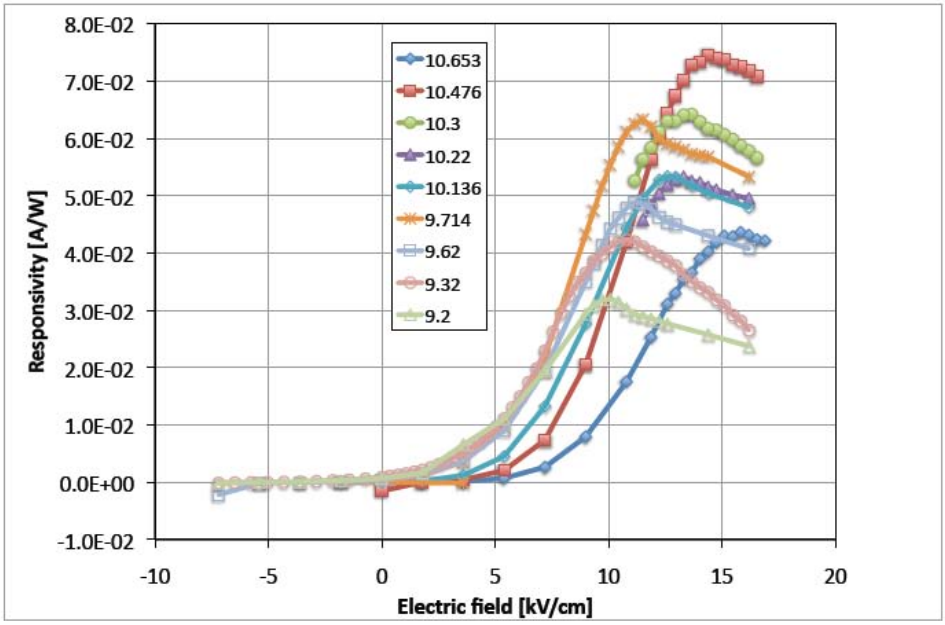

Figure 3: 77 K photoconductivity versus bias and wavelength (microns) for V121049T at $\sim$9 W/cm^2 incident intensity. Power drift from the CO_2 laser or beam pattern changes combined with position drift results in 10% power uncertainty. Notably moving from 9.7 μm has larger and narrower response relative to nearby wavelengths and 10.6 μm has lower and broader response.

Appendix D: Summary of invention disclosures

1. TA 11043: Laser-triggered electrical switch

This technical advance involves a laser-triggered electrical switch that is based on intersubband electronic transitions within a quantum cascade (QC) structure [Fig. 1 (left)]. An electrically-biased QC structure is used to block the flow of current from a voltage source. As shown in Fig. 1 (right), the switching mechanism involves the absorption and reemission of laser-trigger radiation, resulting in transport of electrons from left to right quantum wells. Unique to this switching scheme is that there is no depletion of trigger.

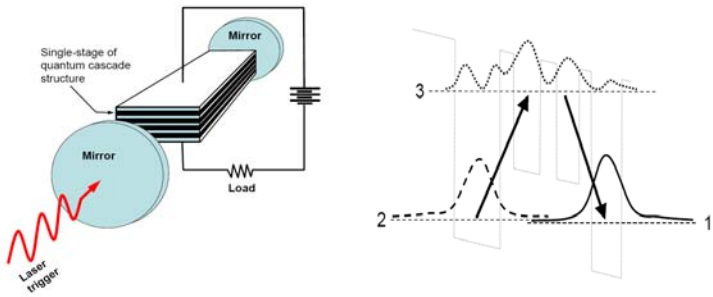

Fig. 1. (Left) Sketch of QC-based laser-triggered electrical switch. (Right) Single stage of laser-triggered electrical switch..

2. TA 11079: Intersubband photomultiplier enabled by photon recycling

This disclosure involves a different approach to achieving amplification than the conventional photomultiplier tube (PMT). Similar to the PMT, a single photon creates multiple electrons at the anode. However, our device is a semiconductor chip [see Fig. 2 (left)] with advantages of low bias voltage, structure ruggedness, radiation hardness and femtosecond response.

As shown in Fig. 2 (right), absorption and subsequent remission of the incident photon (transitions 2-3 and 3-1, respectively) moves the electron from leftmost quantum well to rightmost quantum well. Upon reaching the rightmost quantum well, the electron is swept to the anode by an electric field created with forward bias, producing a photocurrent. The process recovers the photon, which is then available for transporting more electrons

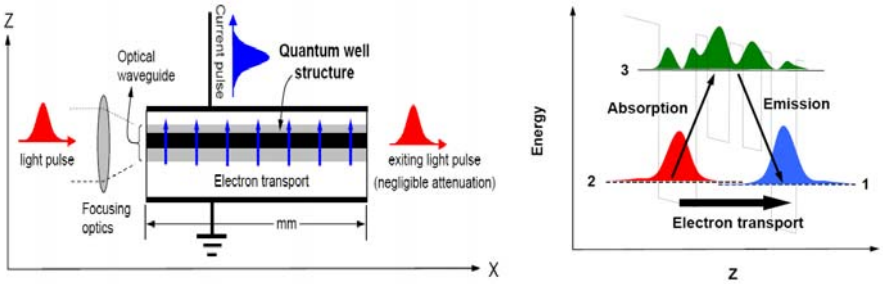

Fig. 2. (Left) Sketch of intersubband photomultipilier. (Right) Absorption followed by emission of incident photon creates a photocurrent.

3. TA 11318: Radiation-brightness enhancer

Disclosure is for enhancing coherence of a radiation field with a semiconductor structure [Fig. 3 (left)]. Device converts incoherent input radiation into spectrally narrower and more collimated output beam, using a multi-quantum-well structure operating with interband and intersubband transitions [Fig. 3 (right)]. The input field creates conduction electrons via an interband transition, where the electron and hole dispersions provide a broad absorption bandwidth. The output radiation is from an intersubband transition, where the discreteness of the intersubband resonance and a waveguide give spectral narrowing and beam collimation.

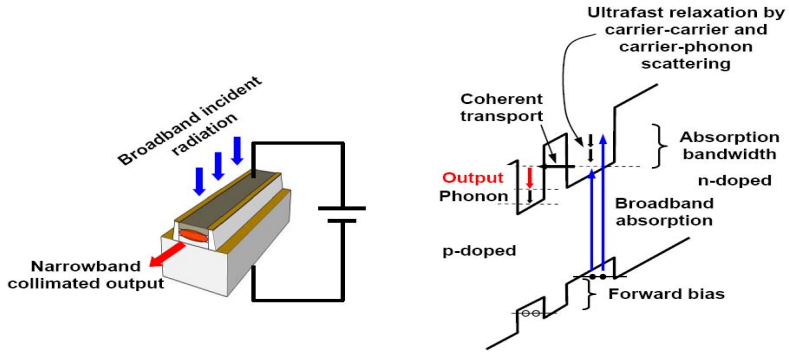

Fig. 3. (Left) Sketch of radiation-brightness enhancer. (Right) Single stage of active medium.

4. TA 11317: Solar-powered high-brightness light source

Disclosure is for high-brightness light sources that are powered by solar radiation. The scheme is based on a quantum well structure that contains two sets of quantum wells. One set is compressively strained and configured to allow broadband absorption of incident solar radiation incident normal or near-normal to the wafer surface. The transition is from valence to conduction subbands. The device also contains a second set of quantum wells that is tensile strained and configured to allow narrowband emission that is collimated by a waveguide that encompasses the entire active region. The emission transition is between conduction subbands. Important to the scheme is that the emitting quantum well, being tensile strained is very weakly absorbing to the incident solar radiation because of polarization selection rules.

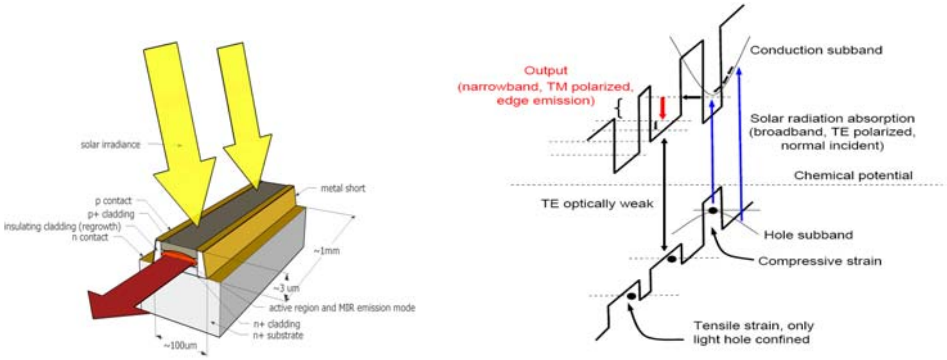

Fig. 4. (Left) Solar-powered high-brightness light source. (Right) Single stage of active medium.

Appendix E: List of invited talks, contributed talks and TAs

Invited talks (International meetings)

W. W. Chow, I. Waldmueller, M. Wanke, *Quantum Coherence in Quantum Cascade Lasers: Paths to THz Generation and Correlated Photon Emission*, 38th Winter Colloquium on The Physics of Quantum Electronics, 1/6-10/08, Snowbird, UT.

W. W. Chow, *Update on our understanding of semiconductor-laser gain: from quantum well to quantum dots.* 39th Winter Colloquium on The Physics of Quantum Electronics, 1/7-11/09, Snowbird, UT (plenary).

M. C. Wanke, ' , '*Monolithic Terahertz Transceivers Integrating QCL's and Schottky Diodes*,' 39th Winter Colloquium on The Physics of Quantum Electronics, 1/7-11/09, Snowbird, UT.

I. Waldmueller, 'Thinking outside the Box: THz QCLs seen differently,' Tera-Mir 2009, Nov3-6 2009, Turkey.

Contributed talks

Waldmueller, I., M. C. Wanke, M. Lerttamrab, W. W. Chow, *Designing THz QCLs Top-Down: Tuning the Emission Frequency of a THz QCL over a Range of 2.9 THz*, International Workshop on Optical Terahertz Science and Technology 2009 (OTST), 3/7-11/09, Santa Barbara, CA.

Waldmueller, I., M. C. Wanke, M. Lerttamrab, D. Allen, W. W. Chow, *Inverse-Quantum-Engineering: A New Methodology for Designing THz QCLs for Basic and Applied Research*, Conference on Lasers and Electro-Optics (CLEO), 5/31-6/5/09, Baltimore, MD.

Waldmueller, W. W. Chow, M. C. Wanke, 'High-Temperature All-Optical Intersubband Terahertz wave switch,' Conference on Lasers and Electro-Optics (CLEO), May 4-9, 2008, Baltimore, MD.

Waldmueller, I., Design emission frequency-dependent comparison of THz QCLs, ITQW 2009, Sept 6-11, 2009 Montreal, Canada

TAs

SD-11079, *Intersubband photomultiplier enabled by photon recycling*, Mike Wanke (1725) and Weng Chow (1123)

SD-11043 *Laser-triggered electrical switch*, Ines Waldmueller (1123), Mike Wanke (1725) and Weng Chow (1123)

SD-11317, *Solar-powered high-brightness light source*, Weng Chow (1123), Mike Wanke (1725) and Dan Allen (1725)

SD- 11318 , *Radiation-brightness enhancer*, Weng Chow (1123), Mike Wanke (1725) and Dan Allen (1725).

SD-11424/S-118609, *Method for Designing Heterostructure Devices*, Mike Wanke (1725), Ines Waldmueller (1123), Weng Chow (1123).

SD-11425, *Intersubband Photon-Avalanche Detector/Amplifier*, Dan Allen (1725), Weng Chow (1123) and Mike Wanke (1725).

SD-11349, *Laser-threat sensor*, Weng Chow (1123), Sebastian Wieczorek (Exceter) and Torrington (5711).

SD-121474 *Microring-resonator variable optical delay*, Zhenshan Yang (1123) and Weng Chow

Appendix F: Final Briefing

4-wave mixing for phase-matching free nonlinear optics in quantum cascade structures (08-0346)

PI Weng Chow (1123), PM Jim Hudgens (1725), FY08-10, $1200K

Purpose, Goals and Approach:

Advance THz optoelectronics

Understand & apply intersubband nonlinear optics

Approach Theory and experiments on conduction state transitions

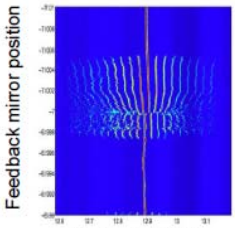

QCL feedback sensitivity

Significance of Results:

Acheived physics understanding useful for development of new and improved THz QCLs at Sandia

Developed quantum-optics tools enabling study of nonclassical-light devices (applications: quantum computing, secure communication, ...).

Key Accomplishments:

- Improved understanding of QCL dynamics and optical nonlinearities
- Introduced ideas for intersubband and intersubband-interband devices
- Initiated bandstructure optimization scheme
- Initiated exploration of semiconductor quantum optics
- 7 TA's, 7 papers (refereed journals), 1 plenary and 3 invited talks at international meetings
- New customers: Enh Surety (C5) Adv R&D, BES (PVC, solid-state lighting)

What Next?

Optoelectronics involving control of spontaneous emission leading to nonclassical-light sources.

Prediction of possibility of strong light–matter interaction in silicon

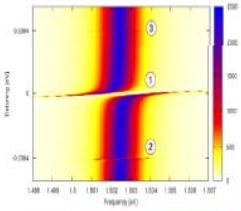

1 Sandia National Laboratories

Which SMU(s) will benefit from this R&D, and over what time frame ?

- ST&E, DSA
- Remote sensing (2 to 5 years)
  SD-11317, *Solar-powered high-brightness light source,*
  SD- 11318 , *Radiation-brightness enhancer*
  SD-11349, *Laser-threat sensor*
- THz technology (2 to 5 years)
  SD-11424/S-118609, *Method for Designing Heterostructure Devices*
  SD-11043 *Laser-triggered electrical switch*
- Spontaneous emission control: Nonclassical light sources (5 to 15 years)
  Phys. Rev. Lett. **104**, 156801, 2010.

What is the impact/legacy of this project?

- Positioned Sandia to be a player in the next wave of advances in quantum electronics and quantum optics (nonclassical light sources and detectors)
- Scientific developmental opportunities (esp. for young staff members: Waldmueller, Tauke-Pedretti, Shaner, Yang)

Sandia National Laboratories

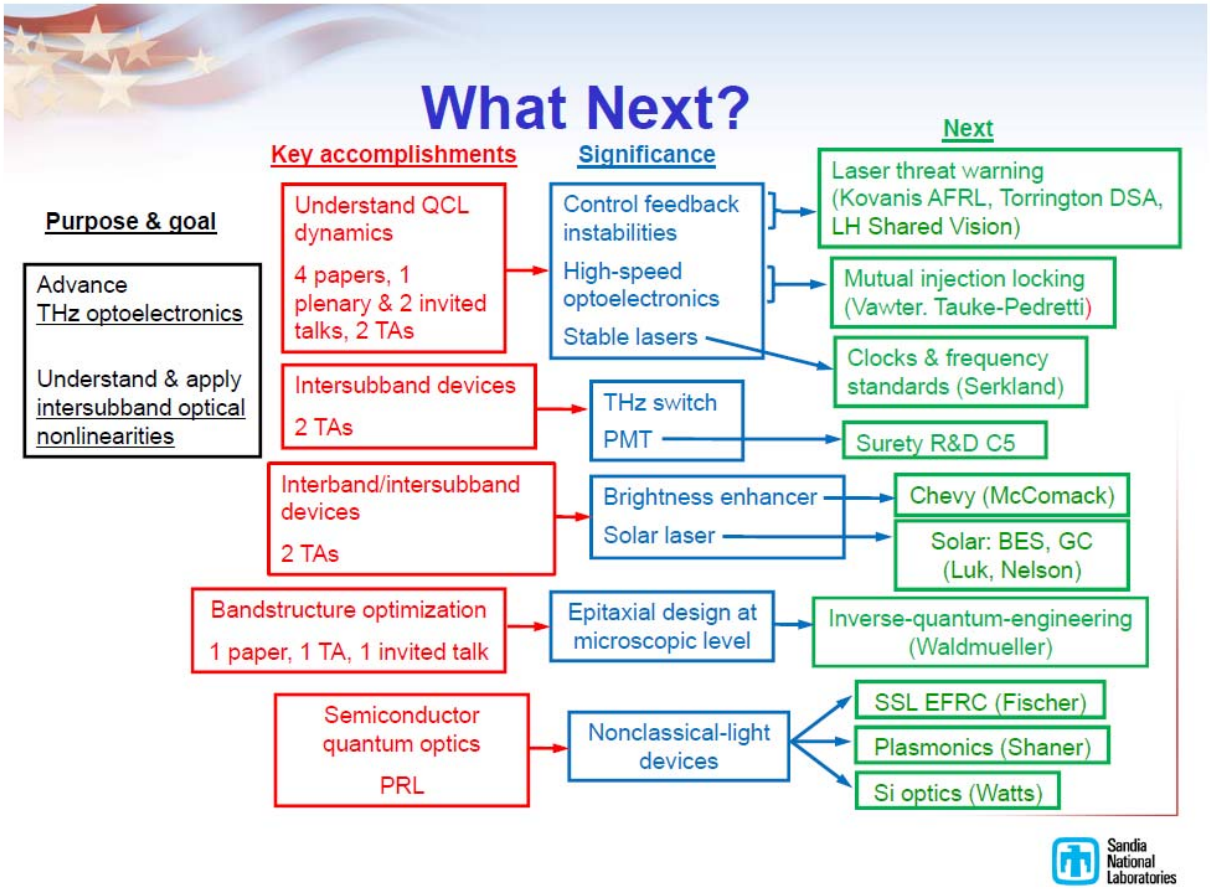
What Next?
Purpose & goal
Advance THz optoelectronics
Understand & apply intersubband optical nonlinearities
Key accomplishments
Understand QCL dynamics
4 papers, 1 plenary & 2 invited talks, 2 TAs
Intersubband devices
2 TAs
Interband/intersubband devices
2 TAs
Bandstructure optimization
1 paper, 1 TA, 1 invited talk
Semiconductor quantum optics
PRL
Significance
Control feedback instabilities
High-speed optoelectronics
Stable lasers
THz switch
PMT
Brightness enhancer
Solar laser
Epitaxial design at microscopic level
Nonclassical-light devices
Next
Laser threat warning (Kovanis AFRL, Torrington DSA, LH Shared Vision)
Mutual injection locking (Vawter. Tauke-Pedretti)
Clocks & frequency standards (Serkland)
Surety R&D C5
Chevy (McComack)
Solar: BES, GC (Luk, Nelson)
Inverse-quantum-engineering (Waldmueller)
SSL EFRC (Fischer)
Plasmonics (Shaner)
Si optics (Watts)
Sandia National Laboratories

Refereed journals

W. W. Chow and S. Wieczorek, 'Using chaos for remote sensing of laser radiation,' Optics Express **17**, 7491-7504, 2009.

S. Wieczorek and W. W. Chow, 'Bifurcations and chaos in a semiconductor laser with coherent or noisy optical injection,' Optics Commun. **282**, 2367, 2009.

A. Carmele, M. Richter, W. W. Chow and A. Knorr, 'Antibunching of thermal radiation by a room-temperature phonon bath: a numerially solvable model for a strongly interacting light-matter-reservoir system,' Phys. Rev. Lett. **104**, 156801, 2010.

In`es Waldmueller, Michael C. Wanke, Maytee Lerttamrab, Dan G. Allen, and Weng W. Chow, ' Inverse-Quantum-Engineering: A New Methodology for Designing Quantum Cascade Lasers,' IEEE J. Quantum Electron. 46, 1414, 2010.

Z. Yang, A.Tauke-Pedretti, G. A. Vawter, and W. W. Chow, 'Mechanism for modulation response improvement in mutually injection-locked semiconductor lasers,' (accepted IEEE JQE).

J. Kabuss, Alexander Carmele, M. Richter, W. W. Chow and A. Knorr, 'Inductive equation of motion approach for a semiconductor QD-QED: coherence induced control of photon statistics,' (accepted physica status solidi).

D. G. Allen, T. W. Hargett, J. L. Reno and M. C. Wanke , 'Optical bistability from domain formation in terahertz quantum cascade lasers,' (accepted IEEE J. Selected Topics in Quantum Electron.)

Invited talks (International meetings)

W. W. Chow, I. Waldmueller, M. Wanke, *Quantum Coherence in Quantum Cascade Lasers: Paths to THz Generation and Correlated Photon Emission,* 38th Winter Colloquium on The Physics of Quantum Electronics, 1/6-10/08, Snowbird, UT.

W. W. Chow, *Update on our understanding of semiconductor-laser gain: from quantum well to quantum dots.* 39th Winter Colloquium on The Physics of Quantum Electronics, 1/7-11/09, Snowbird, UT (plenary).

M. C. Wanke, ' , '*Monolithic Terahertz Transceivers Integrating QCL's and Schottky Diodes,*' 39th Winter Colloquium on The Physics of Quantum Electronics, 1/7-11/09, Snowbird, UT.

I. Waldmueller, 'Thinking outside the Box: THz QCLs seen differently,' Tera-Mir 2009, Nov3-6 2009, Turkey.

TAs

SD-11079, *Intersubband photomultiplier enabled by photon recycling*, Mike Wanke (1725) and Weng Chow (1123)

SD-11043 *Laser-triggered electrical switch*, Ines Waldmueller (1123), Mike Wanke (1725) and Weng Chow (1123)

SD-11317, *Solar-powered high-brightness light source,* Weng Chow (1123), Mike Wanke (1725) and Dan Allen (1725)

SD- 11318 , *Radiation-brightness enhancer,* Weng Chow (1123), Mike Wanke (1725) and Dan Allen (1725).

SD-11424/S-118609, *Method for Designing Heterostructure Devices*, Mike Wanke (1725), Ines Waldmueller (1123), Weng Chow (1123).

SD-11425, *Intersubband Photon-Avalanche Detector/Amplifier,* Dan Allen (1725), Weng Chow (1123) and Mike Wanke (1725).

SD-11349, *Laser-threat sensor*, Weng Chow (1123), Sebastian Wieczorek (Exceter) and Torrington (5711)

SD- *Microring-resonator variable optical delay*, Zhenshan Yang (1123) and Weng Chow (1123). (in preparation)

Contributed talks

Waldmueller, I., M. C. Wanke, M. Lerttamrab, W. W. Chow, *Designing THz QCLs Top-Down: Tuning the Emission Frequency of a THz QCL over a Range of 2.9 THz,* International Workshop on Optical Terahertz Science and Technology 2009 (OTST), 3/7-11/09, Santa Barbara, CA.

Waldmueller, I., M. C. Wanke, M. Lerttamrab, D. Allen, W. W. Chow, *Inverse-Quantum-Engineering: A New Methodology for Designing THz QCLs for Basic and Applied Research,* Conference on Lasers and Electro-Optics (CLEO), 5/31-6/5/09, Baltimore, MD.

Waldmueller, W. W. Chow, M. C. Wanke, 'High-Temperature All-Optical Intersubband Terahertz wave switch,' Conference on Lasers and Electro-Optics (CLEO), May 4-9, 2008, Baltimore, MD.

Waldmueller, I., Design emission frequency-dependent comparison of THz QCLs, ITQW 2009, Sept 6-11, 2009 Montreal, Canada

Sandia National Laboratories

OPED Results

- Designed and tested first generation of OPED structures.
  - Learned that even weak tunnel coupling will lock the structure into the wrong bias conditions at low temperature
  - Could release the tunnel lock by heating the structure until thermally induced leakage exceeds tunnel current
  - Saw frequency dependent photoresponse, negative currents, and interesting time dependent photocurrent.
  - Found that the conduction band offset had to be modified slightly to get agreement with absorption data.
  - Designed and grew structures to provide better data regarding the actual conduction band offset which is critical to this project
- Due to growth issues could not grow another 2-aluminum ratio design for remainder of project.
  - Redesigned structures to minimize tunnel coupling issues while trying to use only 1 aluminum ratio.
  - Came up with PMT concept - initially as way to test pumping efficiency in various designs - spun this into another program to explore photon recycling to improve detector response. (Also submitted TA).
- Lost MBE growth for significant time - developed MOCVD growth capability to create these types of structures (required significant modifications to existing growth parameters).
  - Tested MOCVD growth results and provided feedback by measuring many calibration absorption samples
  - Measured photoresponse of multiple samples (mostly MOCVD grown) which allowed us to reduce tunnel coupling, reduce thermal avalanche, increase the photocurrent, and align the pumping transition with the available pump laser energy.
- Did not see THz emission yet. But we're unable to test the last sample designed after all the calibrations, growth development and design enhancements were incorporated.
  - Have received requests from H.C.Liu to send samples so that he can try final measurements.
  - Have also received requests from Manfred Giehler for further modelling support of their independent efforts at experimental realization of these devices.

Sandia National Laboratories

Distribution: (all electronic copies)

MS 0359	D. Chavez, LDRD Office	1911
MS 1086	W. W. Chow	1123
MS 1086	D. L. Barton	1123
MS 1314	I. Waldmueller	1123
MS 1086	Z. Yang	1123
MS 1802	M. Wanke	1725
MS 0114	D. Allen	1931
MS 0899	Technical Library	9536

Sandia National Laboratories